Magnetism of iron oxide based core-shell nanoparticles from interface mixing with enhanced spin-orbit coupling

E. Skoropata,[1,*] R. D. Desautels,[1] C.-C. Chi,[2] H. Ouyang,[2] J. W. Freeland,[3] and J. van Lierop[1,†]

[1]*Department of Physics and Astronomy, University of Manitoba, Winnipeg, MB, R3T 2N2, Canada*

[2]*Materials Science and Engineering, National Tsing Hua University, Hsinchu, Taiwan*

[3]*Advanced Photon Source, Argonne National Laboratory, Argonne, Illinois 60439, USA*

(Received 14 August 2013; revised manuscript received 28 November 2013; published 13 January 2014)

We show that the magnetism of core-shell nanoparticles (made of maghemite, γ-Fe_2O_3, cores and transition-metal and metal-oxide shells) is altered substantially by the interface, which is a doped iron-oxide layer formed naturally during the seed-mediated synthesis process, a route used typically to produce core-shell nanoparticles. Characteristics fundamental to useful applications, such as the anisotropy and superparamagnetic blocking temperature, were altered substantially with Cu, CoO, MnO, and NiO shells. To ascertain the origin of this behavior, the prototype γ-Fe_2O_3/CoO core-shell nanoparticles are described in detail. We show that the magnetism originates essentially from an interfacial doped iron-oxide layer formed via migration of shell ions, e.g., Co^{2+}, into octahedral site vacancies in the surface layers of the γ-Fe_2O_3 core. For this system, an overall Fe $m_{orb}/m_{spin} = 0.15 \pm 0.03$ is measured ($m_{orb} \sim 0$ for the Fe-oxides) and an enhanced Co $m_{orb}/m_{spin} = 0.65 \pm 0.03$ elucidates the origin of the unexpectedly high overall anisotropy of the nanoparticle. This interfacial layer is responsible for the overall (e.g., bulk) magnetism and provides a perspective on how the magnetism of core-shell nanoparticles manifests from the selected core and shell materials.

DOI: 10.1103/PhysRevB.89.024410 PACS number(s): 75.75.−c, 61.46.Df, 76.80.+y, 78.70.Dm

I. INTRODUCTION

The sensitivity of nanoparticle properties to small changes in composition and morphology that alter the band structure and local atomic environment via quantum confinement effects has motivated increasingly complex nanomaterials. Of considerable interest currently is the core-shell type nanoparticle.[1,2] Multiple phases with complimentary properties combined with a fine control of size provide phenomena unattainable in single-phase nanomaterials.[3] In particular, through direct modification of the core-shell interfacial interactions stem substantial improvements to the overall anisotropy, exchange bias, and superparamagnetic blocking behavior.[4] The fabrication of these nanomaterials is by the deliberate selection of magnetically distinct core and shell materials and has been most notably implemented by researchers investigating ferromagnetic/antiferromagnetic materials with an emphasis on improving the magnetic stability and heat dissipation properties.[5,6] Research into core-shell systems has produced fruitful results. However, the wide variety of magnetism observed in core-shell systems has yet to be explained systematically from a fundamental magnetism viewpoint. An open question that remains: what is the origin of the superior magnetism of core-shell nanoparticles, in particular in relation to the physics at the core-shell interface?

For core-shell nanoparticles, the overall magnetism is considered typically as an interpolation of the intrinsic core and shell magnetism. This description is largely due to the challenges of characterizing interfaces over the germane length scales (often <1 nm, with no large lateral dimension to facilitate measurements as with thin films). Further, core-shell nanoparticles are subject to unique surface and disorder effects, which make comparison with analogous particle/matrix (often containing crystallites or clusters) and thin films (with long range order) challenging. Also, assuming an interpolation of material properties is especially problematic for the ferrites, that are a large fraction of core-shell nanomagnets. A wide range of stoichiometry and composition is accessible by cation substitution, and variations in the degree of inversion and possible vacancies all affect the core-shell interface that can alter the magnetism. Recently, careful characterizations of Fe-oxide/Mn-oxide nanoparticles using elemental and x-ray mapping techniques have shown that an interfacial layer can form.[7,8] While there have been many studies to examine the magnetic role of the interface (e.g., due to roughness, intermixing, and pinning), the relationship between the composition and magnetic configuration at the interface and the overall magnetism of the core-shell nanoparticle resulting from the total of the intrinsic, surface, interface, and disorder effects, remains an open question.

We present a study of maghemite (γ-Fe_2O_3) nanoparticles modified with surface layers of CoO, Cu, MnO, and NiO. γ-Fe_2O_3 was chosen as it offers the largest amount of site disorder and vacancies of the ferrites providing the best vehicle to study core-shell magnetism. The core-shell nanoparticles are examined in comparison with high-quality, single-phase γ-Fe_2O_3 seed particles[9] to distinguish the additional effects of the shell from the intrinsic properties of the γ-Fe_2O_3 core. We find that the anisotropy and superparamagnetic blocking temperature are decoupled and influenced strongly by the choice of shell material in a manner not necessarily accountable to the intrinsic properties of the shell material, suggesting that interfacial interactions are responsible for the observed magnetism. As an example, we present one of our detailed studies of the composition and magnetism for these nanoparticles; γ-Fe_2O_3/CoO core-shell particles wherein the effects of the antiferromagnetic CoO shell and Co^{2+} dopant ions can be distinguished clearly and enable the core-shell interface sharpness to be examined. We show that the overall magnetic properties of the γ-Fe_2O_3/CoO nanoparticles are inconsistent with the existence of a two-layer configuration that is commonly used to describe core-shell nanoparticles.

We provide a self-consistent description of the magnetism and composition at "bulk"/overall, atomic, and elemental scales to identify definitively an intermixed layer formed by Co^{2+} migration into the vacant octahedral sites of the γ-Fe_2O_3 core to form Co-doped γ-Fe_2O_3 interface while maintaining a pure γ-Fe_2O_3 core. The overall magnetic properties are dominated by this interfacial layer via coupling of the Fe^{3+} and Co^{2+} with enhanced moments.

II. EXPERIMENT

A. Preparation of core-shell nanoparticles

The core/shell nanoparticle synthesis was a two part process. The γ-Fe_2O_3 cores were synthesized as described in Ref. 10. A precursor of metal-cupferronate was prepared for each shell material using $CoCl_2{\cdot}6H_2O$ (98%, Alfa Aesar), $MnCl_2{\cdot}4H_2O$ (99%, Arcos Organics), $Ni(CH_3COO)_2{\cdot}4H_2O$ (99%, Acros Organics), and cupferron ($NH_4[C_6H_5N(O)NO]$, 99%, Acros Organics) using the procedure outlined in Ref. 11. A precursor solution containing 1.8 mmol of metal-cupferronate in octylamine (99%, Acros Organics) was heated to 373 K in an argon atmosphere. To add the shells, 4 mL of the precursor were injected rapidly into 7 mL of γ-Fe_2O_3 nanoparticle solution that had been heated to 523 K in an argon atmosphere. The entire mixture was heated to 498 K for 30 minutes, then the reaction was stopped by cooling the system to room temperature. Powder samples used for x-ray diffraction (XRD), Mössbauer spectroscopy, and polarized x-ray experiments were obtained by mixing the nanoparticle stock solution with alcohols to remove excess surfactant, and air drying.

B. Experimental techniques

Transmission electron microscopy (TEM) images were collected using a JEOL 2100F. The nanoparticles were prepared by dropping a mixture of nanoparticle solution diluted in hexanes onto a copper coated carbon grid.

X-ray powder diffraction patterns were collected using a Brüker D8 DaVinci with CuKα radiation using Bragg-Brentano geometry under ambient conditions. The diffraction patterns were collected using dried nanoparticle samples on a zero-background quartz slide using a rotating stage. Lattice parameters for the core and shell were determined using a Rietveld refinement using FULLPROF.[12]

X-ray absorption spectroscopy (XAS) and x-ray magnetic circular dichroism (XMCD) measurements were done at beamline 4-ID-C of the Advanced Photon Source in a liquid helium cryostat with powder samples mounted on carbon tape onto a cold finger in a 7 T (maximum) field magnet. All XMCD spectra were collected in total electron yield mode and are XAS normalized.

Transmission Mössbauer spectra were collected from 10 to 300 K using a Janis SHI-850 closed cycle refrigeration system and a WissEl constant acceleration spectrometer with a 10 GBq ^{57}Co**Rh** source. The source drive velocity was calibrated using a 6-μm-thick α-Fe foil at room temperature.

Magnetometry experiments were done using samples prepared from 20 μL of nanoparticle stock solution dispersed in 50 mg of paraffin wax to ensure similar particle separation.[13] Magnetometry and susceptometry experiments were performed using a Quantum Design magnetic properties measurement system (MPMS XL-5). Hysteresis loops were measured from 5 to 300 K from $\pm$5 T after cooling in a 5 T field. Zero-field cooled (ZFC)/field cooled (FC) dc susceptibility measurements were done from 5 to 300 K using 0.1 mT applied field, and ac susceptibility measurements were done using a 0.025 mT oscillating applied field from 10 Hz to 1 kHz from 5 to 300 K.

III. RESULTS AND DISCUSSION

A. Composition and microstructure

All of the XRD patterns contained [e.g., Fig. 1(e)] reflections characteristic of the spinel structure ($Fd\bar{3}m$) with lattice parameter ~8.36 Å, which is expected for γ-Fe_2O_3 or a doped-γ-Fe_2O_3.[14,15] Additional reflections due to the coating materials were observed for all patterns; components with the rock-salt structure ($Fm\bar{3}m$) with lattice parameters of 4.212 $\pm$ 0.002 Å, 4.401 $\pm$ 0.002 Å, and 4.195 $\pm$ 0.002 Å

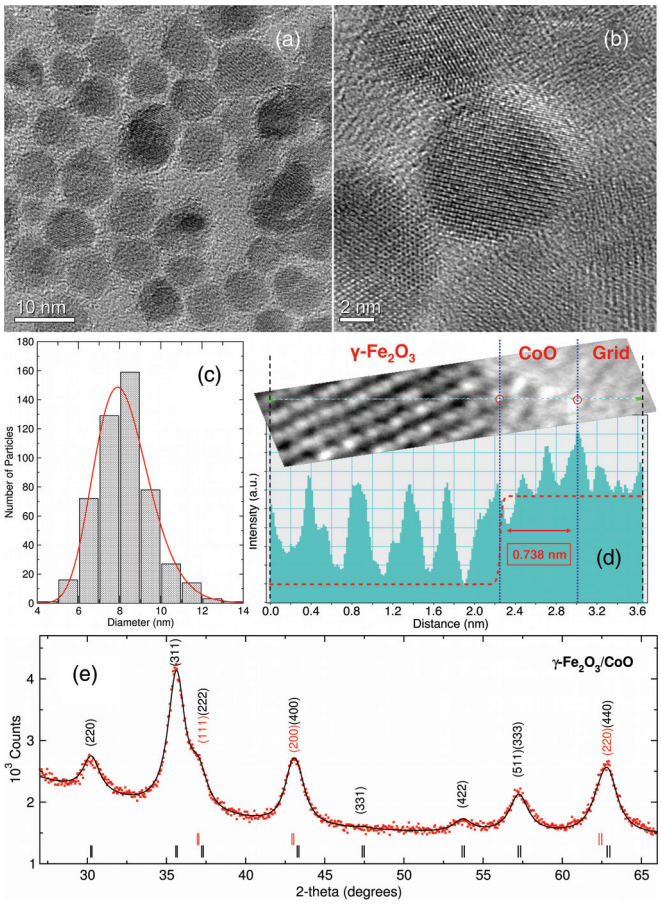

FIG. 1. (Color online) (a) A typical TEM image used to determine the γ-Fe_2O_3/CoO size distribution. (b) HRTEM image of a γ-Fe_2O_3/CoO particle. (c) The size histogram from 500 nanoparticles and log-normal fit (solid line), (d) The analysis to determine the CoO shell thickness from the HRTEM image intensity profile with the lattice fringes, and (e) XRD pattern of γ-Fe_2O_3/CoO nanoparticles, with the results of the refinement (black line) and Bragg markers for γ-Fe_2O_3 (black) and CoO (red).

were observed for the CoO, MnO, and NiO shells, respectively, and the $Fm\bar{3}m$ phase of Cu with a lattice parameter of 3.61 ± 0.02 Å was observed for the Cu shell.[16] Electron diffraction patterns were in agreement with the XRD results. Transmission electron microscopy images revealed that the nanoparticles were of the core-shell type (i.e., not nanoparticle mixtures) with CoO, MnO, and Cu forming complete shell layers, and the NiO forming a "spotted" surface layer. While the γ-Fe_2O_3/NiO nanoparticles did not contain a complete surface shell, γ-Fe_2O_3 and NiO were in chemical contact and, as a result, would be subject to similar intermixing effects as the other nanoparticles investigated, although the lack of a structurally coherent NiO layer may alter the magnetism of the core-shell nanoparticle. As an example of the particle sizes (Fig. 1), we observed a log-normal size distribution for the γ-Fe_2O_3/CoO nanoparticles, with a mean diameter (D) of 7.9 ± 0.1 nm and $\ln(\sigma)$ of 0.07 ± 0.01 [Fig. 1(c)]. These results confirmed that the shell increased the overall particle size relative to the γ-Fe_2O_3 seed particles ($D = 6.6 \pm 0.1$ nm).[17] The shell thickness was measured directly using the electron contrast between core and shell materials with HRTEM images [Fig. 1(b)]. The intensity profile of the core and shell lattice fringes provided a thickness of 0.7 ± 0.2 nm [Fig. 1(d)]. Similar results were observed for the other coating materials.

B. Magnetometry and susceptometry

A magnetic hysteresis loop is the conventional way to characterize the magnetic anisotropy that is a measure of energy barrier to magnetization reversal. The coercivity $[H_C = (H_{C1} - H_{C2})/2]$ is measured as the applied magnetic field required to reverse the sample magnetization (see Fig. 2).

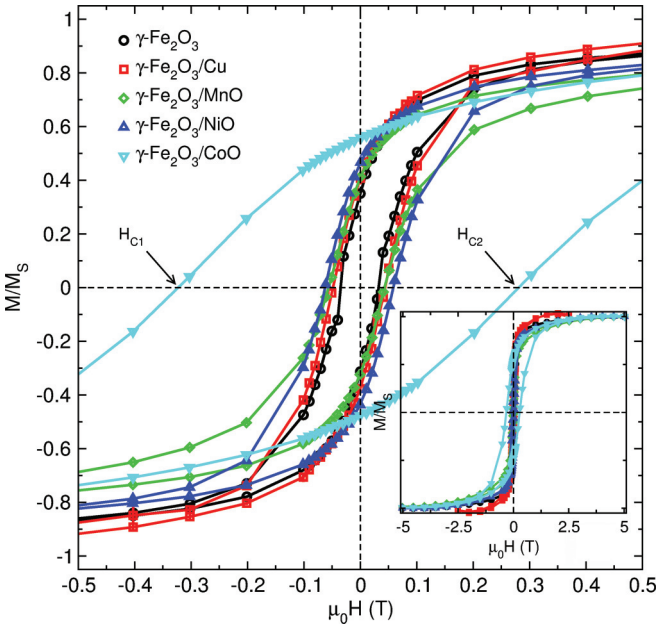

FIG. 2. (Color online) (a) Hysteresis loops collected at 5 K for γ-Fe_2O_3 (black ◯), γ-Fe_2O_3/Cu (red □, from Ref. 16 for comparison), γ-Fe_2O_3/MnO (green ◇), γ-Fe_2O_3/NiO (blue △), and γ-Fe_2O_3/CoO (cyan ▽). The inset shows the full ±5 T field scan.

TABLE I. Coercivity (H_C), exchange bias (H_{EX}) at 5 K, and an estimate of the superparamagnetic blocking temperature (T_B) from dc and ac susceptibility measurements for γ-Fe_2O_3 and core-shell nanoparticles.

	H_C (mT)	H_{EX} (mT)	T_B (K)
γ-Fe_2O_3	33 ± 1.5	4 ± 1	~150
γ-Fe_2O_3/CoO	298 ± 2	17 ± 2	~300
γ-Fe_2O_3/Cu	48 ± 2	5 ± 2	~200
γ-Fe_2O_3/MnO	49 ± 1	7 ± 1	~150
γ-Fe_2O_3/NiO	60 ± 1	0 ± 1	~150

Hysteresis loops measured at 5 K after cooling the samples in a 5 T field (to set a preferred orientation of the interface and core magnetization) revealed that the anisotropy of the core-shell nanoparticles was increased relative to uncoated γ-Fe_2O_3 regardless of the coating material used and that a substantial increase in H_C resulted from the addition of a CoO shell. An exchange bias loop shift $[H_{EX} = (H_{C1} + H_{C2})/2]$ is observed when the magnetization has a preferred orientation from a unidirectional anisotropy due to interfacial magnetic interactions, and is characterized by a shift in the hysteresis loop along the field axis. In uncoated γ-Fe_2O_3, an exchange bias is observed due to an interaction between the disordered surface and the ordered core spin populations.[18] The effect of the increase in anisotropy was also observable in the temperature dependence of the dc susceptibility and frequency dependent ac susceptibility measurements with T_B estimated from the frequency dependence of the maximum in the ac susceptibility and the divergence of the FC and ZFC dc susceptibilities (e.g., Fig. 3 for uncoated γ-Fe_2O_3 and γ-Fe_2O_3/CoO). The results of the magnetometry and susceptometry experiments for the core-shell nanoparticles are summarized in Table I. In typical FM(FiM)/AFM exchange bias systems, the exchange bias field is a result of a unidirectional anisotropy induced by an interfacial exchange interaction. Among this series of core-shell nanoparticles investigated, an increase in H_{EX} and H_C would be expected for all AFM shells due to the anisotropy contribution for interfacial exchange;[4] an effect observed for the MnO and CoO shells. However, no H_{EX} was measured for the γ-Fe_2O_3/NiO system (a reduction relative to uncoated γ-Fe_2O_3), despite a relatively large H_C (larger than γ-Fe_2O_3/MnO, which had a similar T_B). While the relatively low anisotropy of NiO and the incomplete layer formation may account for a lack of increased H_{EX} in γ-Fe_2O_3/NiO relative to uncoated γ-Fe_2O_3, it does not account for the total disappearance of H_{EX}. Also, if no interfacial exchange is effected by NiO, the larger H_C can not be accounted for by a simple interfacial exchange interaction. The addition of a nonmagnetic Cu shell also resulted in an increase in H_C and T_B relative to uncoated γ-Fe_2O_3 and a reduction and quenching of H_{EX} with increasing Cu thickness.[17] Clearly, the magnetometry results indicate that the core-shell nanoparticles do not conform to the expectations of simple exchange bias (for the AFM shells), or composite (for Cu) systems.

An examination of the magnetometry data for the γ-Fe_2O_3/CoO nanoparticles (Fig. 4) supports the determination that the core-shell systems do not display properties of a typical two-layer (exchange bias) system. For example, the

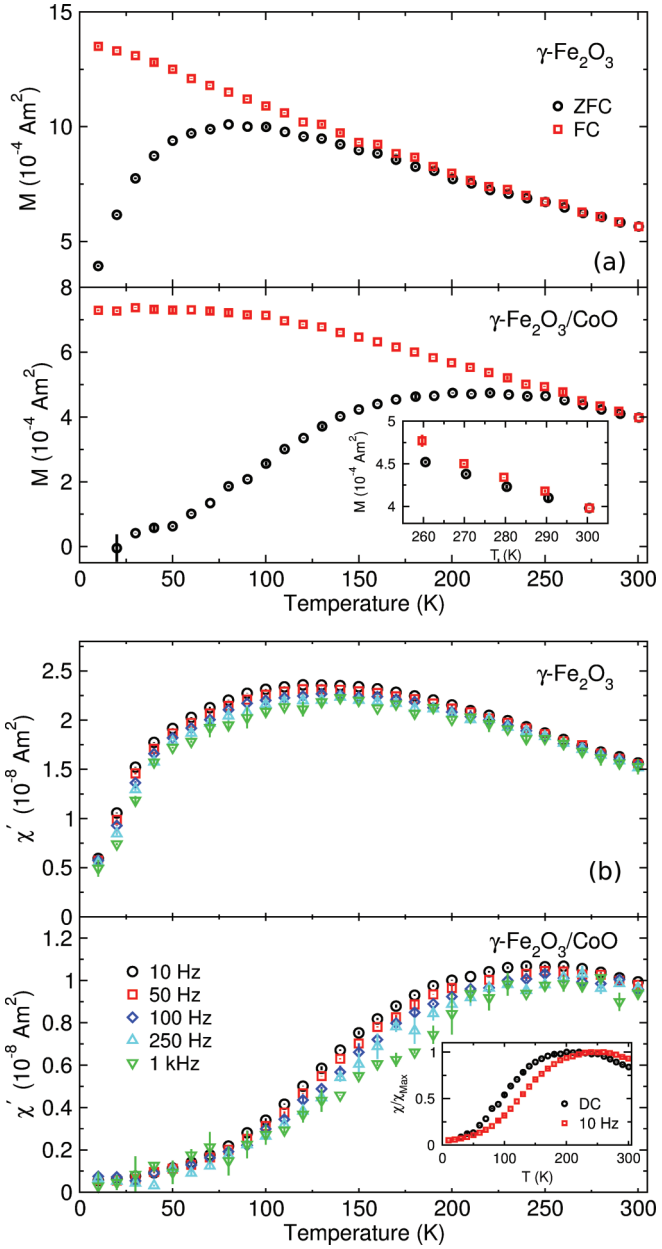

FIG. 3. (Color online) (a) Zero-field cooled (ZFC)/field cooled (FC) dc susceptibility, where the inset shows the high temperature region, and (b) ac susceptibility, where the inset shows the ZFC dc and 10 Hz ac susceptibility curves which have been normalized to the maximum values, for comparison. Results are shown for γ-Fe_2O_3 (top) and γ-Fe_2O_3/CoO (bottom).

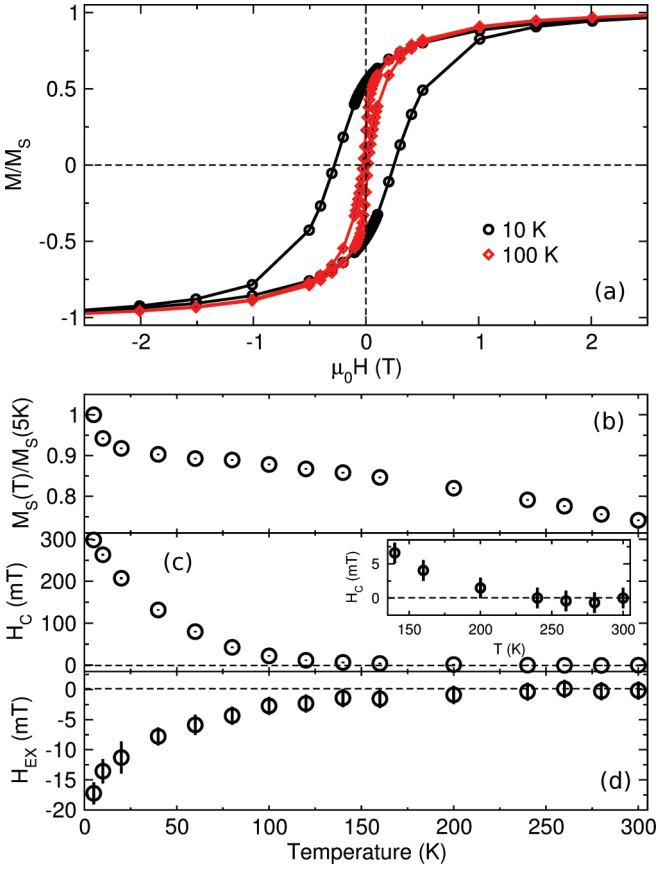

FIG. 4. (Color online) (a) Hysteresis loops for γ-Fe_2O_3/CoO at 10 K (black ◯) and 100 K (red ◇), and the temperature dependence of the (c) saturation magnetization (M_S), (d) coercivity (H_C) showing the full temperature range and temperatures near the onset of H_C (inset), and (e) exchange bias (H_{EX}) for γ-Fe_2O_3/CoO.

hysteresis loops show a clear two-phase shape, observed as a loop narrowing as H_C is approached, shown in Fig. 4(a), that persists until H_C becomes zero at 200 K. This was not observed in the uncoated γ-Fe_2O_3 nanoparticles, and in γ-Fe_2O_3/CoO could be due to magnetically distinct core and intermixed phases, each with a different effective anisotropy. The discrepancy between the low frequency ac susceptibility and ZFC dc susceptibility curves, which show different curve maxima and shapes, shown in the inset of Fig. 3(b), also suggests contributions from multiple spin populations. The temperature dependence of the saturation magnetization[19] for γ-Fe_2O_3/CoO [Fig. 4(a)] shows clearly an exponential-like behavior at the lowest temperatures that is due to the freezing of disordered surface spins that is also observed in the uncoated γ-Fe_2O_3 cores.[18] In the γ-Fe_2O_3/CoO core-shell nanoparticles, this population appears with the same relative weight as in the γ-Fe_2O_3 cores indicating that the surface spin disorder from the core persisted in the core-shell nanoparticle. Interestingly, by contrast, for γ-Fe_2O_3/Cu with a similar shell thickness the disordered population is eliminated.[17]

The difference in anisotropy between the γ-Fe_2O_3/CoO and uncoated γ-Fe_2O_3 is observed clearly by comparing the temperature dependence of H_C for the systems, which do not coincide even when rescaled to the respective T_B values for the onset of H_C, as shown in Fig. 5. This indicates that the H_C difference is due to a change in the particle anisotropy and not the relative T_B differences. For a uniaxial anisotropy, the temperature dependence of H_C can be described by $H_C = \frac{2K}{M_S}[1 - (\frac{T}{T_B})^{1/2}]$, where K is the effective anisotropy constant for the nanoparticle and M_S is the saturation magnetization. Using an estimate of the volume normalized M_S[13] (where the same nanoparticle volume fraction is expected for all magnetometry samples) $K \sim 2.2 \times 10^4$ J/m^3 was measured for the uncoated γ-Fe_2O_3 cores, which was

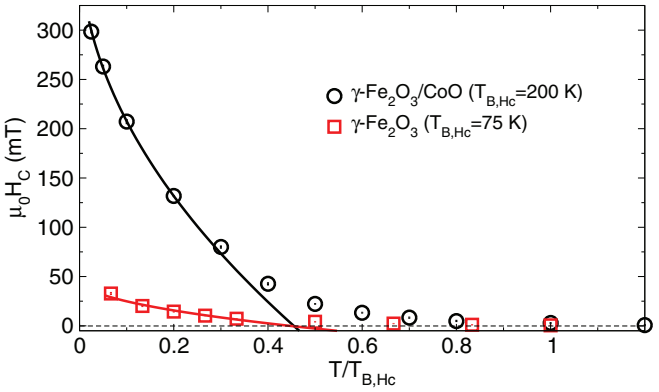

FIG. 5. (Color online) Temperature dependence of the coercivity for uncoated γ-Fe_2O_3 (black ◯) and γ-Fe_2O_3/CoO (red □), with the temperature scaled to onset temperature for the coercivity (T_{B,H_c}) for each sample. The lines indicate a fit to the data as described in the text.

consistent with our previous work,[18] and value typical of γ-Fe_2O_3 nanoparticles. A substantially enhanced $K \sim 1.2 \times 10^5$ J/m^3 was measured for γ-Fe_2O_3/CoO. Since the effective anisotropy of a composite system is typically determined by the component with the largest K, this represents a larger overall increase in K than would be expected from CoO alone (with $K = 5 \times 10^4$ J/m^3).[20] Overall, the increase in H_C and T_B that we observed were significantly higher than has been reported for other mixed γ-Fe_2O_3 and Co nanoparticle systems such as surface cobalt-doped γ-Fe_2O_3[21,22] and composites of similar size γ-Fe_2O_3 and CoO nanoparticles.[23] Since surface doping has a maximum effect at approximately the Co amount required to form a monolayer of (Co,Fe)-oxide at the nanoparticle surface,[22] this suggested that the properties we observed were due to a combination of interfacial exchange with CoO and intermixing effects. To compare the temperature dependent properties, a substantial H_{EX} due to the CoO shell was observed up to 140 K [Fig. 4(c)]. It is reasonable for the T_N of the CoO shell to be reduced substantially relative to the bulk T_N of 290 K considering the shell thickness of ~0.7 nm.[24] However, this also indicates that CoO did not contribute to the persisting H_C above 140 K [see Figs. 4(c) and 4(d)], further demonstrating the existence of an additional magnetic phase. By comparison, no H_{EX} or H_C was observed above 100 K for the uncoated γ-Fe_2O_3 cores.

Altogether the magnetometry data indicate the existence of a high anisotropy phase within the nanoparticle secondary to the γ-Fe_2O_3 core, inconsistent with a simple γ-Fe_2O_3/CoO configuration and suggesting that some core-shell intermixing occurred. However, the magnetometry work has the substantial limitation of being insensitive to the exact source of the measured properties (i.e., H_C, H_{EX}, and T_B), and rather indicates the overall characteristics of the material resulting from the sum total of the intrinsic properties, surface, disorder, and interfacial effects, masking the behavior of each constituent part. As such, although suggesting the existence of an intermixed layer, the nature (i.e. composition and magnetism) of the layer itself is not yet established. A reasonable conclusion to account for the observed magnetism is that a mixed Co-oxide/Fe-oxide layer was formed, likely due to the ease with which the spinel structure will accept dopant cations. Some similar magnetometry results have been obtained in Fe-oxide based core-shell systems, which prompts a more detailed investigation of intermixing effects. If present, in order to understand and manipulate the properties of core-shell nanoparticles (and to understand the magnetism observed in the core-shell series considered herein, and in the literature) this intermixed layer must first be identified and the arrangement of atoms at the interface determined precisely.

C. Atomic magnetism

To better understand the origin of the change in overall magnetism of the core-shell nanoparticles indicated by the magnetometry measurements, the atomic ^{57}Fe magnetism was measured using Mössbauer spectroscopy. Mössbauer spectroscopy uses the resonant absorption and recoilless emission of γ-rays to excite transitions in the probe nuclei. The atomic-level electronic and magnetic environments of ^{57}Fe atoms throughout the sample volume are characterized by the hyperfine parameters that affect the energy required to excite the transitions; specifically, the hyperfine field (B_{hf}) that describes the magnetic environment, the isomer shift (δ), and quadrupolar splitting (Δ) that detail the local electronic environment and the spectrum linewidth (Γ) due to the lifetime of the excited state of the nucleus. For nanoparticles, the onset of superparamagnetism results in a collapse of the spectrum from sextet [e.g., Fig. 6(a)] to singlet since $B_{hf} \rightarrow 0$ with increasing 180° spin flip rates. With the direct measure of the atomic Fe magnetism and a measuring time (~10 MHz) substantially shorter than magnetometry and susceptometry experiments, the effects of magnetic relaxation (e.g., superparamagnetism) are observed more clearly and a more precise determination of T_B is made. For instance, the magnetometry measurements provide only the total sample magnetization and can not distinguish the effects of multiple phases, but rather a distribution of anisotropy barriers within the sample are observed as a broadened maximum in the ac and ZFC dc susceptibilities. In multiple-phase systems where several distinct magnetic components exist attributing a single T_B to the composite system can be problematic. Mössbauer spectroscopy, however, measures directly the contribution from magnetically distinct phases that are characterized by different hyperfine parameters. The Mössbauer spectrum for γ-Fe_2O_3/CoO [Fig. 6(b)] shows a clear static magnetic component at 300 K. Since this is above the T_N of CoO, this effect can not be due to an exchange interaction with the CoO shell. A similar static magnetic population was observed in the Mössbauer spectra for Cu shells at 300 K,[17] and these results suggested strongly that interface mixing is likely a significant factor in determining the magnetism of the core-shell nanoparticle.

A Mössbauer spectrum of γ-Fe_2O_3/CoO at 10 K (well below T_B, to ensure spin dynamics were absent) was used to ascertain the Fe-oxide composition definitively [Fig. 6(a)]. Approximately 75% of the spectrum was comprised of two components with hyperfine parameters[25] typical of the tetrahedral Fe^{3+} A-site, and octahedral Fe^{3+} B-site of γ-Fe_2O_3.[26] The broadened linewidth identified chemical and structural disorder about the Fe sites, typical for γ-Fe_2O_3 nanoparticles.

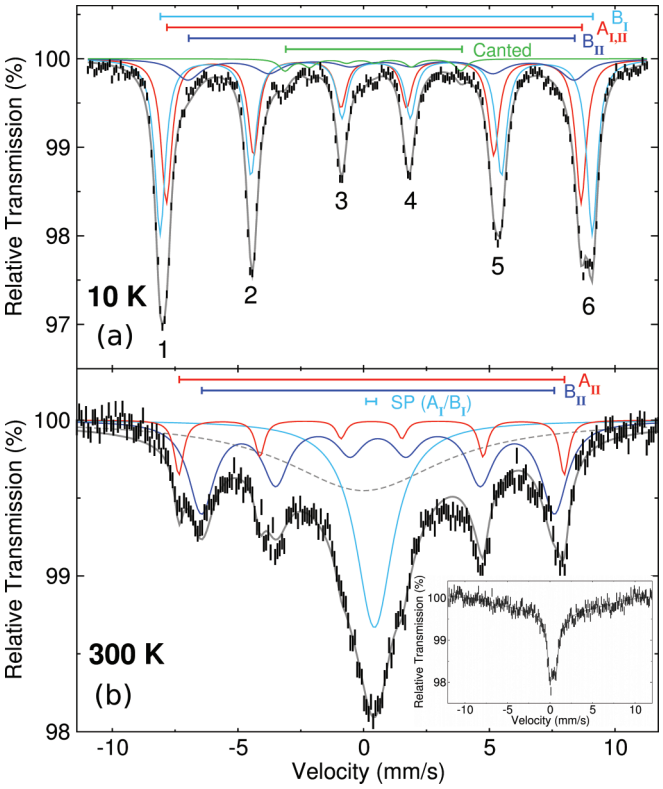

FIG. 6. (Color online) (a) 10 K Mössbauer spectrum of γ-Fe_2O_3/CoO nanoparticles. The numbers mark the spectral lines from the transitions between the $\pm\frac{3}{2} \rightarrow \pm\frac{1}{2}$ nuclear spin states and (b) 300 K Mössbauer spectrum of γ-Fe_2O_3/CoO and γ-Fe_2O_3 (inset). Subspectra labeled I indicate pure γ-Fe_2O_3, and II indicate Co-doped γ-Fe_2O_3.

Approximately 5% of the spectrum area described the low velocity features ($\sim \pm 3$ mm/s) from canted spins due to broken coordination that caused an electric field gradient, Δ,[27] not present in bulk γ-Fe_2O_3.[28]

Interestingly, ~20% of the 10 K spectrum could not be described by stoichiometric γ-Fe_2O_3, and the static portion of the 300 K spectrum [shown in Fig. 6(b)] contained two *resolved* sextets with significantly different hyperfine parameters and Γ's, (measured as the FWHM), inconsistent with γ-Fe_2O_3. This dramatic change in spectral symmetry (visible most clearly by comparing lines 1 and 6 between the 10 and 300 K spectra) was tracked from 10 to 300 K with 25 K intervals. B_{hf} and δ of each component were obtained by incorporating a broad singlet to describe the superparamagnetic component [labeled SP in Fig. 6(b)], and a broad singlet to account for the lineshape effects of magnetic relaxation (although the physics of the process is not described, e.g., magnetic relaxation[9] masked with $\Gamma \sim 0.8$ mm/s versus $\Gamma_{nat} = 0.13$ mm/s). Examining the evolution of the Mössbauer spectra in this way ensured a consistent description of the hyperfine parameters with temperature for each spectral component. The pure γ-Fe_2O_3 component exhibited similar temperature evolution to that of the γ-Fe_2O_3 seed particles[9] [e.g., shown in the inset of Fig. 6(b)]. As such, the broad singlet labeled SP in the 300 K spectrum was identified clearly as from a superparamagnetic pure γ-Fe_2O_3 core, and the presence of a second magnetically distinct phase was confirmed. The remaining ~20% at 10 K, and the change in spectral lineshape asymmetry required a component with significantly larger δ and smaller B_{hf}[29] than the A and B sites of pure γ-Fe_2O_3 that were strikingly similar to the B site of a Co-doped Fe_3O_4.[30,31] This result would be expected for Co-doped γ-Fe_2O_3, since the two structures would differ only by the amount of octahedral site vacancies. The δ measured for the Co-doped Fe-oxide phase indicated the presence of Fe^{2+}, which would be required to maintain charge balance within the structure. As the spectral area represented by each component is proportional to the number of Fe atoms, the A/B site occupancy for each phase can be surmised; the pure γ-Fe_2O_3 components were in good agreement with the expected A/B of 0.375/0.625, and the A/B occupancy of the Co-doped Fe-oxide phase was unchanged from that of the core. The identical occupancies indicated that Co^{2+} substituted into the vacant octahedral sites in γ-Fe_2O_3 at the γ-F_2O_3/CoO interface, rather than displacing Fe^{3+}. Assuming the Fe content was unchanged throughout the core, from the relative spectral areas for the components observed we estimate the core diameter to be 6.1 nm and the interfacial Co-doped layer thickness to be ~0.3 nm from, indicating that only the first few monolayers of the core were affected.

In light of the clear identification of the two Fe-oxide phases, and taking into account the substantially different measuring times for Mössbauer spectroscopy (10^{-8}–10^{-9} s) and magnetometry measurements (10–100 s) a rescaling of the dynamical freezing behavior showed clearly that the H_C up to 200 K was not due to the pure γ-Fe_2O_3 core. Using simple arguments based on the Néel relaxation model, and a typical moment reversal attempt time of 10^{-9}–10^{-11}s, a conservative estimate of the difference in $T_{B,dc}/T_{B,Moss} \sim 2$–4 is expected. That is, for a magnetometry (dc) T_B of 200–250 K (a lower estimate for the γ-Fe_2O_3/CoO system), a completely magnetically split Mössbauer spectrum should be observed at 300 K. However, Fig. 6(b) shows clearly that the pure γ-Fe_2O_3 component was collapsed. The pure γ-Fe_2O_3 component of the Mössbauer spectra shows nearly identical relaxation behavior to uncoated γ-Fe_2O_3 cores that we have examined previously,[9] where $H_C = 0$ above 75 K, and consistent with the rescaling argument. Based on this information, we can conclude that above 75 K the pure γ-Fe_2O_3 component does not contribute to the overall magnetism of the nanoparticle. By contrast, the Co-doped γ-Fe_2O_3 component showed little reduction in B_{hf} relative to the 10 K spectrum and showed almost no additional line broadening (observed clearly in line 1, with a sharp A-site linewidth), characteristic of being below the onset temperature of significant relaxation effects. This means that, in addition to altering the basic characteristics of the nanoparticle magnetism at low temperatures by enhancing H_{EX} and altering the surface spin disorder of the core (as observed in the overall magnetic properties among the series examined), the intermixed layer can also determine completely the magnetism at high temperatures when the low anisotropy γ-Fe_2O_3 core is superparamagnetic.

D. Elemental magnetism

To further understand the evolution of the Fe and Co electronic and magnetic states, x-ray absorption spectroscopy

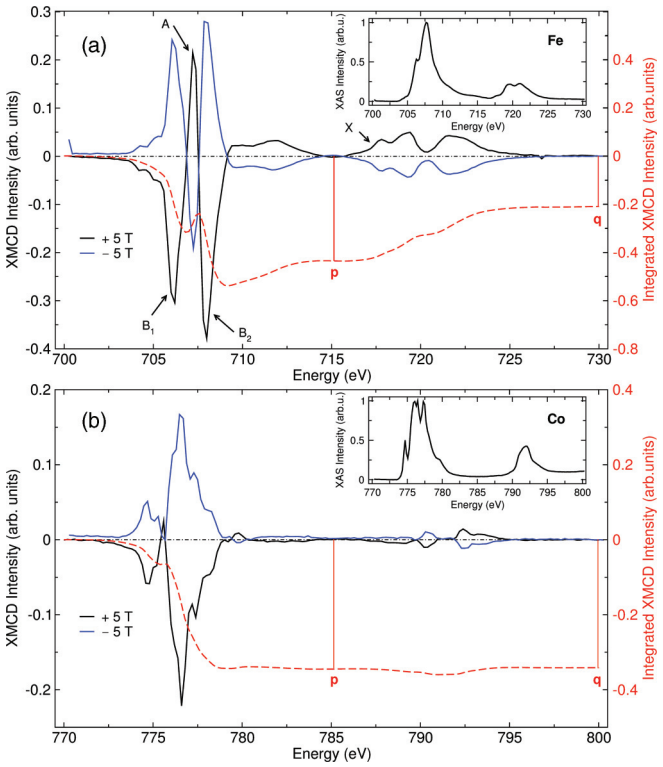

FIG. 7. (Color online) XMCD and XAS (inset) spectra collected over the L_3 and L_2 edges of (a) Fe and (b) Co of γ-Fe_2O_3/CoO nanoparticles at 10 K in ±5 T. The integrated XMCD intensities are shown in the dashed lines (red), with p and q defined in the text.

(XAS) collected over the Fe (700–730 eV) and Co (770–800 eV) $L_{2,3}$ ($2p \rightarrow 3d$ transition) edges (Fig. 7) characterized the coordination environments of the core and shell elements. The Fe XAS spectrum was typical for a spinel Fe-oxide.[32] The Co XAS spectrum was consistent with Co^{2+} in an octahedral environment such as CoO or the octahedral sites of a Co-doped spinel Fe-oxide[33] and differed clearly from that of Co_3O_4,[34] which contains tetrahedrally coordinated Co^{2+}. X-ray magnetic circular dichroism (XMCD) spectra were collected with circularly polarized x-rays quantify the spin and orbital contributions to the magnetic moment. The difference in absorption between left and right circularly polarized x-rays produced an XMCD spectrum with an intensity that was directly proportional to the element and site specific magnetization. For spinel Fe-oxides, which are ferrimagnetic, the magnetic moments *within* the A (tetrahedral) and B (octahedral) sublattices are coupled ferromagnetically (J_{AA}, $J_{BB} > 0$), while the A and B sublattices are coupled antiferromagnetically ($J_{AB} < 0$). The antiparallel orientation of the A- and B-sublattice magnetizations splits the L_3 absorption edge into three lines whose intensities are affected by the amounts of tetrahedral Fe^{3+} (A), octahedral Fe^{2+} (B_1), and octahedral Fe^{3+} (B_2) [Fig. 7(a)], shown by experimental studies of mixed Fe_3O_4 and γ-Fe_2O_3 systems and supported by multiplet calculations that simulate the spectra of individual sites.[32,35] Visually, in the Fe XMCD spectrum for the γ-Fe_2O_3/CoO nanoparticles, the relative B_1/B_2 intensity resembled more closely γ-Fe_2O_3; however, we also observed clearly a small peak at the Fe L_2 edge (~717 eV, labeled X) not observed in pure γ-Fe_2O_3,[32] which suggested that some octahedral Fe^{2+} was present, in agreement with the Mössbauer spectra. Experimentally, an $I_{B1}/I_{B2} \sim 1.38$ and $I_A/I_{B2} \sim 0.4$ are observed for Fe_3O_4, and an $I_{B1}/I_{B2} \sim 0.4$ and $I_A/I_{B2} \sim 0.58$ are observed for γ-Fe_2O_3.[36] The measured $I_{B1}/I_{B2} = 0.804$ and $I_A/I_{B2} = 0.569$ for γ-Fe_2O_3/CoO further supported our determination of an overall Fe composition intermediate to the two Fe-oxides, and nearer to γ-Fe_2O_3. For an antiferromagnet, no XMCD signal is expected since there is no overall magnetization. However, a clear Co XMCD signal indicated a measurable Co magnetization aligned with the octahedral Fe B-sites. This would be expected for Co ions incorporated into the octahedral sites of the ferrimagnetic γ-Fe_2O_3.

The mechanism of the increased anisotropy was revealed by the XMCD spectra for Fe and Co measured in +5 and −5 T (Fig. 7) at 10 K. If all of the ions were able to align with the applied field the +5 T XMCD spectrum should be a perfect mirror image of the −5 T spectrum. However, there was a ~20% increase in the Fe XMCD signal for the +5 T Fe spectrum relative to −5 T, and a similar increase was observed for the Co XMCD signal with the same field polarity dependence. This indicated that there were some spins that did not reorient with reversal of the applied field, and were pinned;[37] we attribute this behavior to an interfacial Fe/Co interaction due to sharing of d-orbitals. Since the orbital and spin moment contribute differently to the L_3 and L_2 edge signals[38,39] the ratio m_{orb}/m_{spin} can be determined from the XMCD spectra using sum rule analysis[40] that results in $m_{orb}/m_{spin}=2q/(9p-6q)$, where p and q are the integrated XMCD intensities over the L_3 edge, and the combined L_3 and L_2 edges, respectively; a total Fe $m_{orb}/m_{spin} = 0.15 \pm 0.03$ and Co $m_{orb}/m_{spin} = 0.65 \pm 0.03$ were observed for the γ-Fe_2O_3/CoO system. These results are consistent with the formation of an interfacial nonstoichiometric Co^{2+}-doped Fe-oxide (which contains magnetic Co^{2+} with a nonzero m_{orb}).[41,42] The relatively large Co m_{orb}/m_{spin} may also be, in part, due to uncompensated Co^{2+} from lower coordination at the interface or CoO shell,[43] or local strain in the interfacial layer.[42] The presence of coupling was also reflected in the enhanced Fe m_{orb}/m_{spin} (m_{orb} is essentially zero for Fe-oxides, even at the nanoscale[44,45]), which has been observed in strained Co-substituted Fe-oxides,[42] and was consistent with the observation of a canted spin population in the Mössbauer spectra, and pinned moments in the XMCD spectra.

IV. CONCLUSION

All of the information shows clearly that the γ-Fe_2O_3-based core-shell nanoparticles do not have a simple two-layer structure but an interfacial doped γ-Fe_2O_3 layer. By characterizing the composition in detail, we identified clearly the presence of an interfacial cobalt doped γ-Fe_2O_3 layer that arose from Co^{2+} migration into vacant octahedral sites at the γ-Fe_2O_3 surface. We have shown that the combined effects of the single ion anisotropy of Co^{2+} in the spinel structure and exchange bias (interfacial coupling) effects have acted cooperatively to increase the total anisotropy of the

nanoparticle. In addition, the intermixed layer determines the magnetism at high temperatures. In the CoO/γ-Fe_2O_3 nanoparticles, the static magnetism at 300 K above CoO's T_N is fully consistent with a cobalt-ferrite-like layer that would have a substantially higher intrinsic anisotropy (due to the unquenched m_{orb} of Co and Fe ions) and T_C,[41,46–48] and the substantially enhanced H_{EX} relative to the uncoated γ-Fe_2O_3 core is typical of an exchange bias system.

An examination of the magnetism of a series of core-shell nanoparticles including γ-Fe_2O_3 nanoparticles with Cu, CoO, MnO, and NiO shells revealed that the conventional two-layer structure was incompatible with the behavior observed, where a departure from typical exchange bias and and composite material changes in H_C, H_{EX}, and T_B occur. The existence of a mixed-oxide interfacial layer provides a new perspective on how the physics of the overall magnetism manifests from selected core and shell materials. We show that the overall properties of the material are *not* determined by a direct interaction between the core and shell, but rather an interaction through an interfacial layer. The effective dominance of the interfacial layer on the magnetism suggests new avenues for the development of novel properties, for example, by treating the surface of the core particles prior to the addition of a shell material to alter the interface chemistry. Finally, this work provides a new perspective on understanding and manipulating the magnetism of core-shell nanoparticles.

ACKNOWLEDGMENTS

The authors thank NSERC and CFI of Canada, and NSC of Taiwan. Use of the Advanced Photon Source at Argonne National Laboratories was supported by the US DOE under contract DE-AC02-06CH11357. The authors also thank Dr. Shen-Chuan Lo of the Material and Chemical Research Laboratories, Industrial Technology Research Institute, Taiwan for his assistance with the TEM measurements.

*eskoropata@physics.umanitoba.ca
†Johan.van.Lierop@umanitoba.ca

[1] L. Carbone and P. D. Cozzoli, Nano Today **5**, 449 (2010).
[2] W. Schärtl, Nanoscale **2**, 829 (2010).
[3] S. Bose, A. R. Bhattacharyya, P. V. Kodgire, A. R. Kulkarni, and A. Misra, J. Nanosci. Nanotechnol. **8**, 1867 (2008).
[4] J. Nogués, J. Sort, V. Langlais, V. Skumryev, S. Suriñach, J. S. Muñoz, and D. Baró, Phys. Rep. **422**, 65 (2005).
[5] V. Salgueiriño-Maceira and M. A. Correa-Duarte, Adv. Mater. **19**, 4131 (2007).
[6] J.-H. Lee, J.-T. Jang, J.-S. Choi, S. H. Moon, S.-H. Noh, J.-W. Kim, J.-G. Kim, I.-S. Kim, K. I. Park, and J. Cheon, Nat. Nanotech. **6**, 418 (2011).
[7] S. Estradé, L. Yedra, A. López-Ortega, M. Estrader, G. Salazar-Alvarez, M. D. Baró, J. Nogués, and F. Peiró, Micron **43**, 30 (2012).
[8] K. L. Krycka, J. A. Borchers, G. Salazar-Alvarez, A. López-Ortega, M. Estrader, S. Estradé, E. Winkler, R. D. Zysler, J. Sort, F. Peiró, M. D. Baró, C.-C. Kao, and J. Nogués, ACS Nano **7**, 921 (2013).
[9] R. D. Desautels, E. Skoropata, and J. van Lierop, J. Appl. Phys. **103**, 07D512 (2008).
[10] J. Rockenberger, E. C. Scher, and A. P. Alivisatos, J. Am. Chem. Soc. **121**, 11595 (1999).
[11] R. S. Bottei and R. G. Schneggenburger, J. Inorg. Nucl. Chem. **32**, 1525 (1970).
[12] J. Rodríguez-Carvajal, Physica B **192**, 55 (1993).
[13] A lower estimate of the interparticle spacing, achieved by assuming complete conversion of ionic Fe (from the precursor solution used during synthesis) into Fe-oxide nanoparticles results in a minimum interparticle spacing of 75 nm, which is approaching the single-particle limit for γ-Fe_2O_3. This criterium can be applied to the core-shell systems where similar a total nanoparticle moment is expected. Since it is unlikely that the nanoparticle growth was 100% efficient (consumed all of the available ionic Fe^{3+}) this is likely an underestimate of the interparticle spacing. It should be noted, however, that the interparticle spacing is the same for all samples investigated, which is justifies our qualitative comparison of the susceptibility results.
[14] C. Pecharromán, T. González-Carreño, and J. E. Iglesias, Phys. Chem. Minerals **22**, 21 (1995).
[15] R. M. Cornell and U. Schwertmann, *The Iron Oxides: Structure, Properties, Reactions, Occurrences and Uses* (Wiley-VCH Verlag GmbH & Co. KGaA, 2003).
[16] R. D. Desautels, E. Skoropata, Y.-Y. Chen, H. Ouyang, J. W. Freeland, and J. van Lierop, Appl. Phys. Lett. **99**, 262501 (2011).
[17] R. D. Desautels, E. Skoropata, Y.-Y. Chen, H. Ouyang, J. W. Freeland, and J. van Lierop, J. Phys.: Condens. Matter **24**, 146001 (2012).
[18] T. N. Shendruk, R. D. Desautels, B. W. Southern, and J. van Lierop, Nanotechnol. **18**, 455704 (2007).
[19] We have not examined the measured saturation magnetization of the sample for several reasons. Firstly, the bulk saturation magnetization of maghemite and substituted oxides are similar and the fraction taken up by the intermixed layer is small. For example, 20% of the Fe-oxide-based core in γ-Fe_2O_3/CoO a Co-doped maghemite-like phase, formed by Co^{2+} migrating into the octahedral site vacancies in the γ-Fe_2O_3 surface layers. Fe^{3+}, which occupies the A- and B-sites of maghemite has a moment of 5 μ_B. Since the A- and B-sublattices are antiferromagnetically coupled, γ-Fe_2O_3 has 2.5 μ_B/f.u. When Co^{2+} (3 μ_B) fills a (previously) vacant octahedral site, two Fe^3 must be converted to Fe^{2+} (4 μ_B) to maintain overall charge balance. As such, a the largest moment that can be achieved from Co substitution is 2.75 μ_B/f.u. For a 20% fraction of intermixed phase, this constitutes a 2% change in the sample magnetization. Secondly, the M_S is expected to vary depending on the surface, disorder, or interface effects which may alter M_S in a less reliably and quantitatively predictable fashion and can not be elucidated directly from the measured M_S value.
[20] R. C. O'Handley, *Modern Magnetic Materials: Principles and Applications* (Wiley, New York, 2000).
[21] M. P. Sharrok, P. J. Picone, and A. H. Morrish, IEEE Trans. Magn. **19**, 1466 (1983).
[22] G. Salazar-Alvarez, J. Sort, A. Uheida, M. Muhammed, S. Suriñach, M. D. Baró, and J. Nogués, J. Mater. Chem. **17**, 322 (2007).
[23] C. Frandsen, C. W. Ostenfeld, M. Xu, C. S. Jacobsen, L. Keller, K. Lefmann, and S. Mørup, Phys. Rev. B **70**, 134416 (2004).

[24]Y. J. Tang, D. J. Smith, B. L. Zink, F. Hellman, and A. E. Berkowitz, Phys. Rev. B **67**, 054408 (2003).

[25]Tetrahedral Fe^{3+} A-site $B_{hf} = 51.25 \pm 0.05$ T, $\delta = 0.402 \pm 0.005$ mm/s; octahedral Fe^{3+} B-site $B_{hf} = 53.42 \pm 0.03$ T, $\delta = 0.500 \pm 0.004$ mm/s; and Γ(FWHM) $= 0.26 \pm 0.01$ mm/s (relative to $\Gamma_{nat} = 0.13$ mm/s for the source).

[26]J. Tuček, R. Zobril, and D. Petridis, J. Nanosci. Nanotechnol. **6**, 926 (2006).

[27]$B_{hf} = 21.7 \pm 0.5$ T, $\Delta = 0.49 \pm 0.05$ mm/s.

[28]F. T. Parker, M. W. Foster, D. T. Margulies, and A. E. Berkowitz, Phys. Rev. B **47**, 7885 (1993).

[29]$B_{hf} = 47.7 \pm 0.1$ T, $\delta = 0.68 \pm 0.03$ mm/s, $\Gamma = 0.6 \pm 0.1$ mm/s.

[30]E. De Grave, R. M. Persoons, R. E. Vandenberghe, and P. M. A. de Bakker, Phys. Rev. B **47**, 5881 (1993).

[31]R. M. Persoons, E. De Grave, P. M. A. de Bakker, and R. E. Vandenberghe, Phys. Rev. B **47**, 5894 (1993).

[32]S. Brice-Profeta, M.-A. Arrio, E. Tronc, N. Menguy, I. Letard, C. Cartier dit Moulin, M. Noguès, C. Chanéac, J.-P. Jolivet, and P. Sainctavit, J. Magn. Magn. Mater. **288**, 354 (2005).

[33]F. M. F. de Groot, M. Abbate, J. van Elp, G. A. Sawatsky, Y. J. Ma, C. T. Chen, and F. Sette, J. Phys.: Condens. Matter **5**, 2277 (1993).

[34]F. Zheng, S. Alayoglu, J. Guo, V. Pushkarev, Y. Li, P.-A. Glans, J.-L. Chen, and G. Somorjai, Nano Lett. **11**, 847 (2011).

[35]E. Pellegrin, M. Hagelstein, S. Doyle, H. O. Moser, J. Fuchs, D. Vollath, S. Schuppler, M. A. James, S. S. Saxena, L. Niesen, O. Rogojanu, G. A. Sawatsky, C. Ferrero, M. Borowski, O. Tijernberg, and N. B. Brookes, Phys. Status Solidi B **215**, 797 (1999).

[36]E. Lee, D. H. Kim, J. Hwang, K. Lee, S. Yoon, B. J. Suh, K. H. Kim, J.-Y. Kim, Z. H. Zhang, B. Kim, B. I. Min, and J.-S. Kang, Appl. Phys. Lett. **102**, 133703 (2013).

[37]H. Ohldag, A. Scholl, F. Nolting, E. Arenholz, S. Maat, A. T. Young, M. Carey, and J. Stöhr, Phys. Rev. Lett. **91**, 017203 (2003).

[38]B. T. Thole, P. Carra, F. Sette, and G. van der Laan, Phys. Rev. Lett. **68**, 1943 (1992).

[39]P. Carra, B. T. Thole, M. Altarelli, and X. Wang, Phys. Rev. Lett. **70**, 694 (1993).

[40]C. T. Chen, Y. U. Idzerda, H.-J. Lin, N. V. Smith, G. Meigs, E. Chaban, G. H. Ho, E. Pellegrin, and F. Sette, Phys. Rev. Lett. **75**, 152 (1995).

[41]J. C. Slonczewski, Phys. Rev. **110**, 1341 (1958).

[42]J. A. Moyer, D. P. Kumah, C. A. F. Vaz, D. A. Arena, and V. E. Henrich, J. Magn. Magn. Mater. **345**, 180 (2013).

[43]A. M. Mulders, H. Loosvelt, A. Fraile Rodríguez, E. Popova, T. Konishi, K. Temst, O. Karis, D. Arvantis, and C. van Haesendonck, J. Phys.: Condens. Matter **21**, 124211 (2009).

[44]V. N. Antonov, B. N. Harmon, and A. N. Yaresko, Phys. Rev. B **67**, 024417 (2003).

[45]H. Béa, M. Bibes, S. Fusil, K. Bouzehouane, E. Jacquet, K. Rode, P. Bencok, and A. Barthélémy, Phys. Rev. B **74**, 020101(R) (2006).

[46]E. Fantechi, G. Campo, D. Carta, A. Corrias, C. de Julián Fernández, D. Getteschi, C. Innocenti, E. Pineider, F. Rugi, and C. Sangregorio, J. Phys. Chem. C **116**, 8261 (2012).

[47]R. A. McCurrie, in *Ferromagnetic Materials Structure and Properties* (Academic Press, London, 1994), p. 123.

[48]G. A. Sawatsky and A. H. Morrish, J. Appl. Phys. **39**, 1204 (1968).